JPE 15-5-11

http://dx.doi.org/10.6113/JPE.2015.15.5.1244
ISSN(Print): 1598-2092 / ISSN(Online): 2093-4718

Stability Enhancement of Four-in-Wheel Motor-Driven Electric Vehicles Using an Electric Differential System

Kada Hartani†, Abdelkader Merah*, and Azeddine Draou**

†,*Electrotechnical Engineering Laboratory, University of Saida, Saida, Algeria
**Department of Electrical Engineering, Islamic University of Madinah, Madinah, Saudi Arabia

Abstract

This paper presents a new multi-machine robust control based on an electric differential system for electric vehicle (EV) applications which is composed of four in-wheel permanent magnet synchronous motors. It is based on a new master–slave direct torque control (DTC) algorithm, which is used for the control of bi-machine traction systems based on a speed model reference adaptive system observer. The use of an electric differential in the design of a new EV constitutes a technological breakthrough. A classical system with a multi-inverter and a multi-machine comprises a three-phase inverter for each machine to be controlled. Another approach consists of only one three-phase inverter for several permanent magnet synchronous machines. The control of multi-machine single-inverter systems is the subject of this study. Several methods have been proposed for the control of multi-machine single-inverter systems. In this study, a new master–slave based DTC strategy is developed to generate an electric differential system. The entire system is simulated by Matlab/Simulink. The simulation results show the effectiveness of the new multi-machine robust control based on an electric differential system for use in EV applications.

Key words: DTC, Electric differential, Electric vehicles, In-wheel motor-driven electric vehicle, MRAS, Multi-machine system, Multi-machine control, Traction application

I. INTRODUCTION

Environmental problems such as global warming, the depletion of fossil fuels, and air pollution are becoming serious. Therefore, electric vehicles (EVs) have attracted a great deal of interest as zero-emission vehicles. EVs have the following advantages [1]:

- The development of in-wheel motors enables individual control of each wheel.
- The generated torque can be measured precisely from the motor current.
- The torque response is rapid.

Some applications in the field of electrical drives require the use of several electric machines and many static converters that have an important place among electromechanical systems. These systems are called multi-machine multi-converter systems (MMSs) [2]. MMSs can be considered as extensions of classical drives. In numerous applications, one motor is controlled by one converter known as a single-machine single-converter system. However, in high-power applications such as traction systems, conveyer lines, and steel processing, two or more machines are fed by one converter. This topology results in a light, highly compact, and low-cost system [3]. This system is called a multi-machine single-converter system. The control of multi-machine single-converter systems is the subject of this study. Several methods have been proposed for the control of multi-machine single-inverter systems. In this case, a master–slave based direct torque control (DTC) strategy is developed to generate the electric differential.

Electric differential is another technology that eliminates traditional mechanical differentials [4]-[6]. This system can reduce the weight and friction loss in a driving train by removing the mechanical differential components and

Manuscript received Jul. 23, 2014; accepted Nov. 7, 2014
Recommended for publication by Associate Editor Sang-Won Yoon.
†Corresponding Author: adraou@yahoo.com
Tel: +213-555196347, University of Saida
*Electrotechnical Engineering Laboratory, University of Saida, Algeria
**Dept. of Electrical and Electronic Eng., University of IUM, Arabia

consequently improving the overall reliability and efficiency during power transmission. The working principle of an electric differential system is similar to that of a traditional mechanical differential system. When an EV is cornering or making a turn, the outer wheels travel longer paths than the inner wheels. This implies that the rotational speed of the outer wheels will be faster than that of the inner wheels. The resulting speed differences between the inner and outer wheels are automatically tuned by an electric differential system.

An advantage of EVs is the possible increase in safety because of the DTC and speed during cornering and risky maneuvers. Electric differential is characterized by the following features: 1) no mechanical link exists between the driven wheels; 2) traction power is separately applied to each wheel by a speed controller, and 3) the speed controller applies minimal power to the inner wheel.

EVs equipped with in-wheel motors are envisioned to be future personal EVs on the basis of their energy efficiency and motion control. Over the past few years, research on motion control, including traction control or yaw stability control, has been conducted to utilize independently driven in-wheel motors [1], [7], [8]. In-wheel electrical motor control [9], [11] is a novel technology that provides fast and accurate torque actuation.

Permanent magnet synchronous motors (PMSMs) have been extensively analyzed as feasible candidates for variable speed EV traction applications [12]. PMSMs exhibit high efficiency when operating at constant speeds in the constant torque region because of their low (copper) losses. Vector control techniques are preferred to improve the dynamic performance of induction motor drives for EV propulsion. An innovative control method called DTC has gained attention for electric propulsion systems [13], [15] because, unlike vector control, it can produce fast torque control of PMSMs and does not require heavy on-line computation.

Sensorless control is an attractive feature in DTC for PMSMs without a speed control loop, in which no position or speed signal is needed for the motor and only an initial position is needed for the PMSMs. However, in high-performance applications, speed control is usually required. In this case, the rotor speed should be detected for feedback. As discussed earlier, the use of speed sensors outweighs the advantages of DTC systems. Many researchers have paid considerable attention to the sensorless method of DTC for PMSMs to eliminate the cost of the speed sensor and to improve the reliability of the driving system.

This paper is organized as follows: To improve the dynamic performance of permanent magnet synchronous in-wheel motors, a DTC based on a speed model reference adaptive system (MRAS) observer is proposed. Simulation results are presented to validate the effectiveness of the proposed sensorless control. Section II introduce a three degrees-of-freedom (3-DOF) yaw plan model to describe the lateral motion in EVs. Section III discusses the design of an electric differential for EVs with four independent in-wheel motors based on the new DTC algorithm. Finally, a series of Matlab/Simulink simulation tests is conducted to evaluate the performance of the proposed sensorless master–slave DTC system applied to electric differentials to improve the stability of in-wheel motor-driven EVs.

II. SENSORLESS DTC WITH A MRAS OBSERVER

A block diagram of a sensorless DTC-PMSM that employs a MRAS as speed estimator is shown in Fig. 1. MRAS based estimators provide the desired state from two different models: the reference model and the adjustable model [16] [20]. The error between the two models is used to estimate the unknown parameter (speed in this case). In the MRAS, only the adjustable model depends on the unknown parameter [21], and the reference model is not dependent on speed. The error signal is fed into an adaptation mechanism to provide the estimated quantity, which is used to tune the adjustable model. A sensorless control algorithm (Fig. 2) is employed in this study. A PMSM is considered as the reference model, and the stator current equations are considered as the adjustable model. The estimated rotor speed is used to tune the adjustable model based on the current equations of the motor. The speed error is continuously monitored to ensure negative feedback and, hence, overall system stability. The current equations of the PMSM are given as:

$$\begin{cases} \dfrac{di_d}{dt} = -\dfrac{R_s}{L_s} i_d + \dfrac{L_q}{L_d} i_q \omega_r + \dfrac{1}{L_s} v_d \\ \dfrac{di_q}{dt} = -\dfrac{R_s}{L_s} i_q - i_d \omega_r - \dfrac{\Phi_f}{L_s} \omega_r + \dfrac{1}{L_s} v_d \end{cases} \tag{1}$$

The above current equations can be rewritten as:

$$\frac{d}{dt}\begin{bmatrix} i_d^{'} \\ i_q^{'} \end{bmatrix} = \begin{bmatrix} -\dfrac{R_s}{L_s} & \dfrac{\omega_r L_q}{L_s} \\ -\dfrac{\omega_r L_d}{L_s} & -\dfrac{\hat{R}_s}{L_s} \end{bmatrix} \begin{bmatrix} i_d^{'} \\ i_q^{'} \end{bmatrix} + \frac{1}{L_s} \begin{bmatrix} v_d^{'} \\ v_q^{'} \end{bmatrix} \tag{2}$$

where:

$$\begin{cases} i_d^{'} = i_d + \dfrac{\Phi_f}{L_d} \\ i_q^{'} = i_q \\ v_d^{'} = v_d + \dfrac{R_s \Phi_f}{L_d} \\ v_q^{'} = v_q \end{cases} \tag{3}$$

Eq. (4) has the speed as a variable which will be used for the adjustable model. A PMSM is used as the reference model and provides i_d and i_q. In this algorithm, the

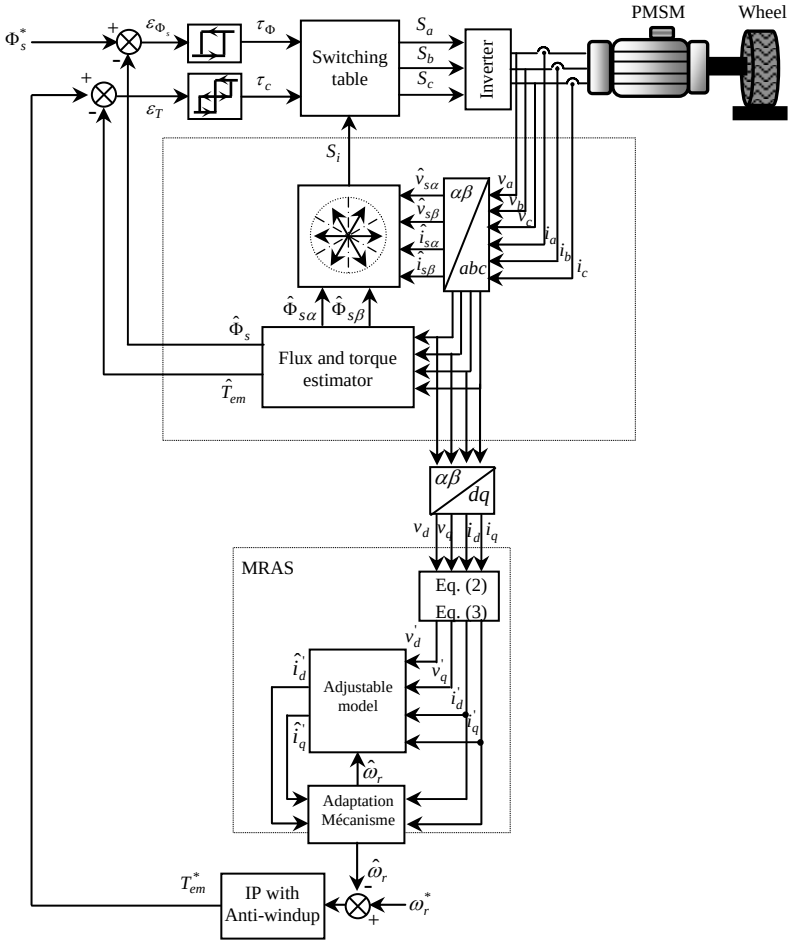

Fig. 1. Block diagram of sensorless DTC-PMSM drive with MRAS based speed estimator.

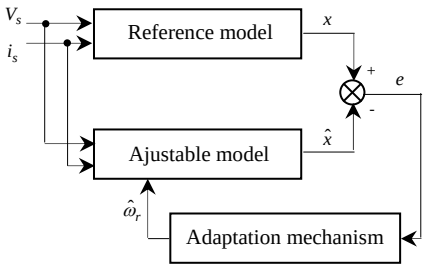

Fig. 2. Structure of the MRAS Block.

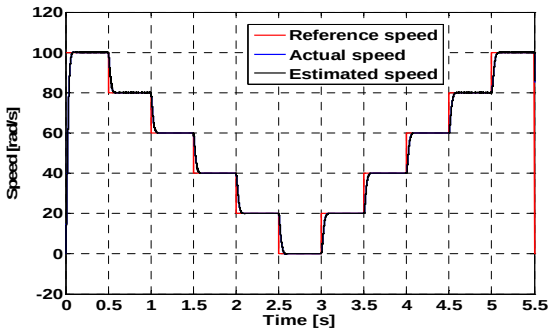

Fig. 3. Sensorless performance for the staircase test.

$$\hat{\omega}_r = k_p + \frac{k_i}{s}\left[-(i'_q - \hat{i}'_q) + (i'_d - \hat{i}'_d) + \hat{\omega}_r(0)\right] \qquad (4)$$

estimated value of the rotor speed is calculated as:

The performance of the MRAS observer is based on the controller used in the adaptation mechanism. In this case, a proportional-integral controller is used to tune the adaptive model based on the reference model. The controller forces the error to be zero. Fig. 3 shows the results of a test in which the sensorless DTC drive is subjected to a stepwise speed changes from 100 rad/s to zero speed in a series of 20 rad/s steps and then back to 100 rad/sec at no load. Fig. 3 indicates that the actual speed and the estimated speed follow the reference speed. Fig. 4 shows a waveform of the speed error between the estimated speed and the actual speed. Fig. 5 shows the sensorless performance during a speed change from 100 rad/s to zero speed at no load. Stable operation and no-oscillating-speed performance are obtained at around the zero speed.

To test the load torque disturbance capability of the sensorless DTC-PMSM drive at low speed, different levels of load torque are applied at 20 rad/s. Fig. 11 shows the

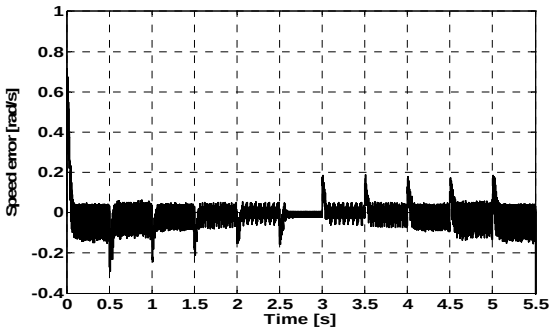

Fig. 4. Error between estimated and actual speeds.

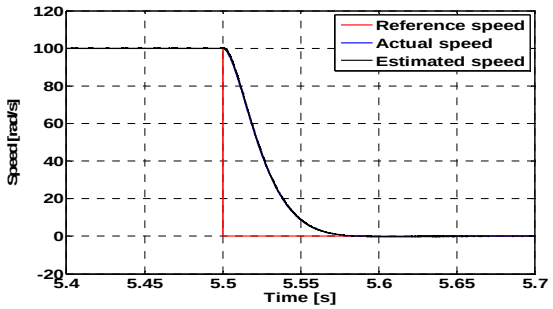

Fig. 5. Estimated and actual speeds at low speeds.

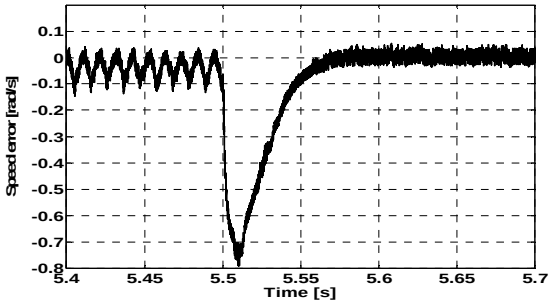

Fig. 6. Error between estimated and actual speeds at low speed.

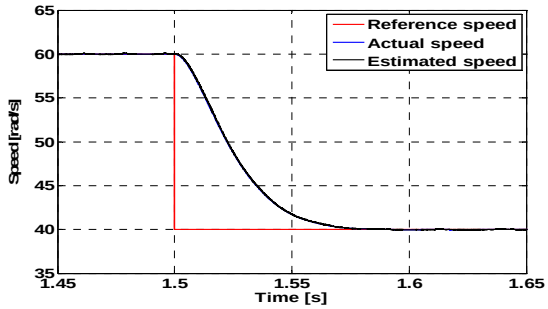

Fig. 7. Sensorless performance for speed change (a) from 60 rad/s to 40 rad/s, and (b) from 40 rad/s to 60 rad/s.

electromagnetic torque generated by the PMSM as a step change in the load torque is applied to the motor. The sensorless performance at low and zero speeds is also good.

III. VEHICLE DYNAMICS

The structure of the EV in this study is composed of four in-wheel motors (i.e., PMSMs) mounted in each wheel, as

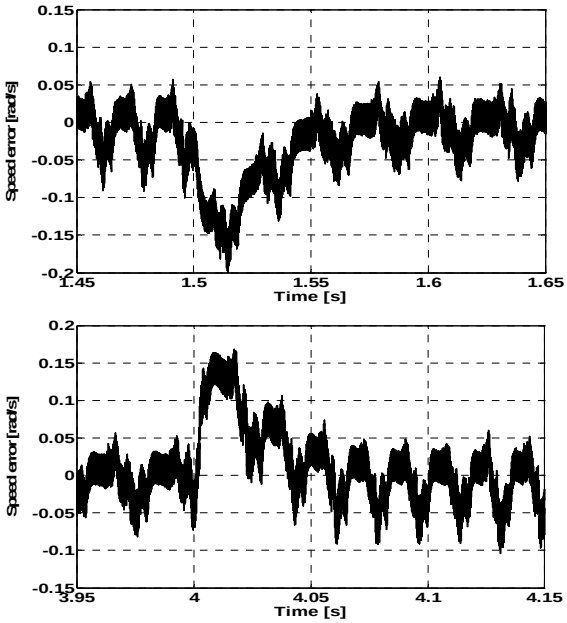

Fig. 8. Error between estimated and actual speeds at low speed.

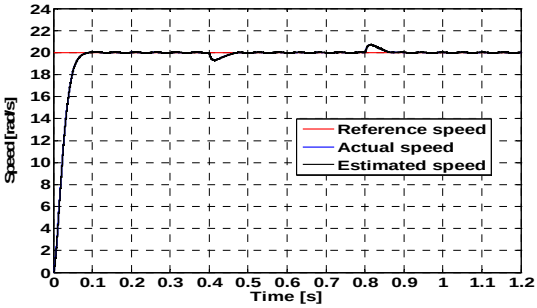

Fig. 9. Sensorless performance for load torque application at 20 rad/s (50% rated load).

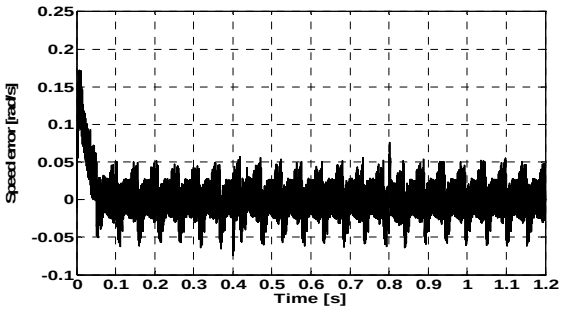

Fig. 10. Error between estimated and actual speeds for load torque application.

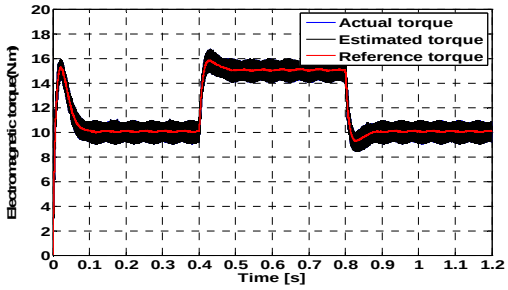

Fig. 11. Electromagnetic torque generated by PMSM.

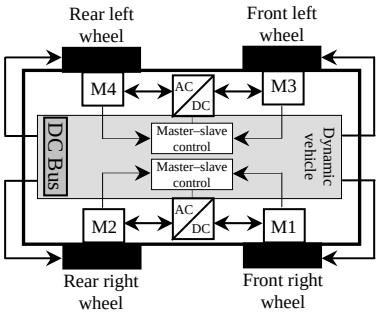

Fig. 12. Configuration of an EV with four independent in-wheel motors.

Fig. 13. In-wheel motors.

shown in Fig. 12 [28]. Therefore, the wheel torque for each wheel can be controlled completely and independently for vehicle motion control. Regenerative braking is also possible.

In this section, a 3-DOF yaw plane model is introduced to describe the lateral motion in EVs. The yaw plane representation is shown in Fig. 14.

The vehicle dynamics are described by the longitudinal velocity, lateral velocity and yaw rate as follows [6], [29], [31] :

$$\begin{aligned}\dot{v}_x &= v_y r + \frac{F_{t1}+F_{t2}+F_{t3}+F_{t4}-F_{res}}{M_v} \\ &\quad + \frac{C_f \delta}{M_v}\left(\frac{v_y + r l_r}{v_x} - \delta\right) \\ \dot{v}_y &= \left(-\frac{C_r + C_f}{M_v v_x}\right) v_y + \left(\frac{C_r l_r + C_f l_f}{M_v v_x} - v_x\right) r + \frac{C_f}{M_v}\delta \\ \dot{r} &= \left(\frac{C_r l_r - C_f l_f}{J_v v_x}\right) v_y - \left(\frac{C_r l_r^2 + C_f l_f^2}{J_v v_x}\right) r + \frac{C_f l_f}{J_v}\delta \\ &\quad + \frac{d}{J_v}\left(F_{t1} + F_{t2} - F_{t3} - F_{t4}\right)\end{aligned}, \quad (5)$$

$$F_{res} = F_{rr} + F_{aero} + F_c, \quad (6)$$

and:

$$\begin{aligned}F_{aero} &= \frac{1}{2}\rho S_f C_{px} V_{cg}^2 \\ F_c &= M_v g \sin(\alpha_p) \\ F_{rr} &= C_{rr} M_v g\end{aligned}. \quad (7)$$

With a linear tire model, the front and rear cornering forces can be expressed as a product of the cornering stiffness (C_f, C_r) and the sideslip angle (α_f, α_r).

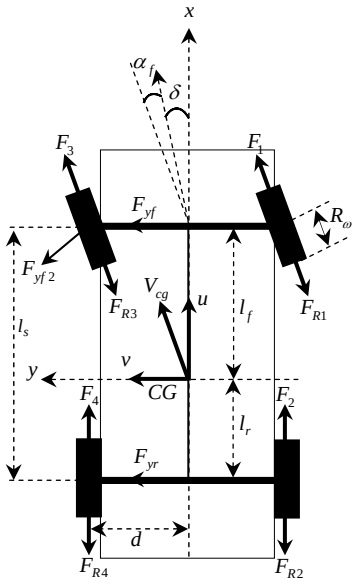

Fig. 14. 3-DOF yaw plane vehicle model.

$$\begin{aligned}F_{yf} &= -C_f \alpha_f \\ F_{yr} &= -C_r \alpha_r\end{aligned} \quad (8)$$

The sideslip angles of the wheels can be easily expressed in terms of the longitudinal, lateral, and angular velocities, as well as the steering angle δ. Explicit expressions of the sideslip angles for the front and rear axles are represented by Eq. (10).

$$\begin{aligned}\alpha_f &= \tan^{-1}\left(\frac{v_y + l_f r}{v_x}\right) - \delta \\ \alpha_r &= \tan^{-1}\left(\frac{v_y - l_r r}{v_x}\right)\end{aligned} \quad (9)$$

The longitudinal slip can be defined for the four wheels as:

$$\lambda_i = \frac{R_\omega \omega_i - u_{ti}}{\max\left(R_\omega \omega_i, u_{ti}\right)}, \; i \in [1,...,4], \quad (10)$$

where:

$i = 1,2,3,$ and 4 correspond to the front left, front right, rear left, and rear right ($= lf, fr, rl, rr$) wheels, respectively; R_ω is the wheel radius; ω_i is the angular velocity of the in-wheel motor; and v is the linear speed at which the contact zone moves on the ground.

The interrelationships between the slip ratio λ and the traction coefficient μ can be described by various formulas. In this study, the widely adopted magic formula [31] [33] is applied to describe the relationship between the slip and traction forces and to build a vehicle model for the following simulations, as shown in Eq. (11).

$$\mu = c_1\left(\sin\left(c_2 \tan^{-1}\left(c_3\lambda - c_4\left(c_3\lambda - \tan^{-1}\left(c_3\lambda\right)\right)\right)\right)\right) \quad (11)$$

The coefficient sets of c_1, c_2, c_3 and c_4 are defined in [31].

The longitudinal forces for the four in-wheel motors can be calculated using the following equation:

$$F_{ti} = \frac{gM_v}{4}\mu_i \cos(\alpha_p)\ ,\ i \in [1,...,4], \tag{12}$$

The drive system model can be described by the following mechanical equations:

$$\begin{aligned} T_{ri} &= F_{ti}R_\omega - N_f d_z \quad ,i \in [1,3] \\ T_{ri} &= F_{ti}R_\omega - N_r d_z \quad ,i \in [2,4] \end{aligned}, \tag{13}$$

where T_{ri} is the resistive torque; N_f, N_r are the front and rear normal forces and have the following expressions:

$$\begin{aligned} N_f &= \frac{M_v g}{2}\left(\frac{l_r}{L} - \frac{h_{cg}}{L_g}\frac{dV_{cg}}{dt}\alpha_p - \frac{h_{cg}}{L}\alpha_p\right) \\ N_r &= \frac{M_v g}{2}\left(\frac{l_f}{L} + \frac{h_{cg}}{L_g}\frac{dV_{cg}}{dt}\alpha_p + \frac{h_{cg}}{L}\alpha_p\right) \end{aligned}, \tag{14}$$

IV. Kinematic and Dynamic Models for the Electric Differential

The electric differential operation supposes the solution of two technological problems: 1) the wheel synchronization and 2) the computation of the relative wheel speed as a function of the turn angle. The relationship between the inner two and outer two wheel velocities in a corner are usually described through the Ackerman steering principle. This principle computes the relative speed differences between the wheels by using the data of the turn (steering) angle. A new DTC algorithm is used to control a bi-machine traction system [22]- [27].

As shown in Fig. 15, the linear velocities of the four wheels are represented by V_{fl}, V_{fr}, V_{rl}, and V_{rr}. The steering angles of the front wheels are shown as δ_{fl} and δ_{fr}. The distances from the front wheels to the rear wheels of the EV [centre of gravity (CG)] are shown as l_f and l_r. Half of the vehicle track is represented by l_s.

When the EV is driven by all four wheels in a cornering maneuver, the inner two wheels and the outer two wheels will have different rotational speeds. On the basis of the kinematic model shown in Fig. 15, the linear velocities of the four wheels are described as follows [34], [35]:

$$\begin{aligned} v_{fl} &= (v_x + rl_s)\cos\delta_{fl} + (v_y + rl_f)\sin\delta_{fl} \\ v_{fr} &= (v_x - rl_s)\cos\delta_{fr} + (v_y + rl_f)\sin\delta_{fl} \\ v_{rl} &= v_x + rl_s \\ v_{rr} &= v_x - rl_s \end{aligned}, \tag{15}$$

The steering angles for the front right and front left wheels are assumed to be the same, namely, $\delta_{fl} = \delta_{fr} = \delta$.

All of the tires are assumed to have the same effective radius R_ω. The reference rotational speed of each wheel

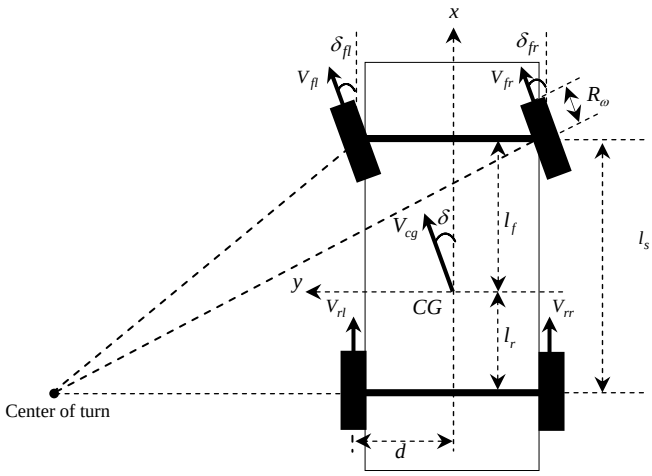

Fig. 15. Kinematic model of an EV in a turn maneuver.

during a turn maneuver is described as follows:

$$\omega_{fl} = \frac{v_{fl}}{R_{e\omega}}, \omega_{fr} = \frac{v_{fr}}{R_\omega}, \omega_{rl} = \frac{v_{rl}}{R_\omega}, \omega_{rr} = \frac{v_{rr}}{R_\omega}, \tag{16}$$

The difference between the angular speeds of the wheel drives is expressed by Eq. (17). The signal of the steering angle indicates the curve direction [Eq. (18)].

$$\Delta\omega = \frac{d.\tan\delta}{l_s}\omega_v^* \tag{17}$$

$$\begin{cases} \delta\rangle 0 \quad \Rightarrow \quad Turn\ \ right \\ \delta = 0 \quad \Rightarrow \quad Straight\ \ ahead \\ \delta\langle 0 \quad \Rightarrow \quad Turn\ \ left \end{cases} \tag{18}$$

When a vehicle arrives at the beginning of a curve, the driver applies a steering angle to the wheels. However, the electronic differential immediately acts on the two motors, reduces the speed of the inner wheel, and increases the speed of the outer wheels. The driving wheel angular speeds are:

$$\omega_l^* = \omega_v^* + \frac{\Delta\omega}{2}, \tag{19}$$

$$\omega_r^* = \omega_v^* - \frac{\Delta\omega}{2}, \tag{20}$$

V. Simulation Results

The objective of the stability control is to improve the vehicle steadiness and transient response properties, thereby enhancing the vehicle handling performance and maintaining stability with regard to maneuvers. The desired vehicle responses are defined on the basis of the concerning intention of the driver (e.g., the steering command and vehicle speed imposed by the driver). The vehicle speed starts from zero to a chosen reference speed of 30 km/h. At this operating point, a cycle variation is imposed on the vehicle chassis by the steering command of the driver, as illustrated in Fig. 17(a). The input hand-steering angle linearly decreases to - 70°

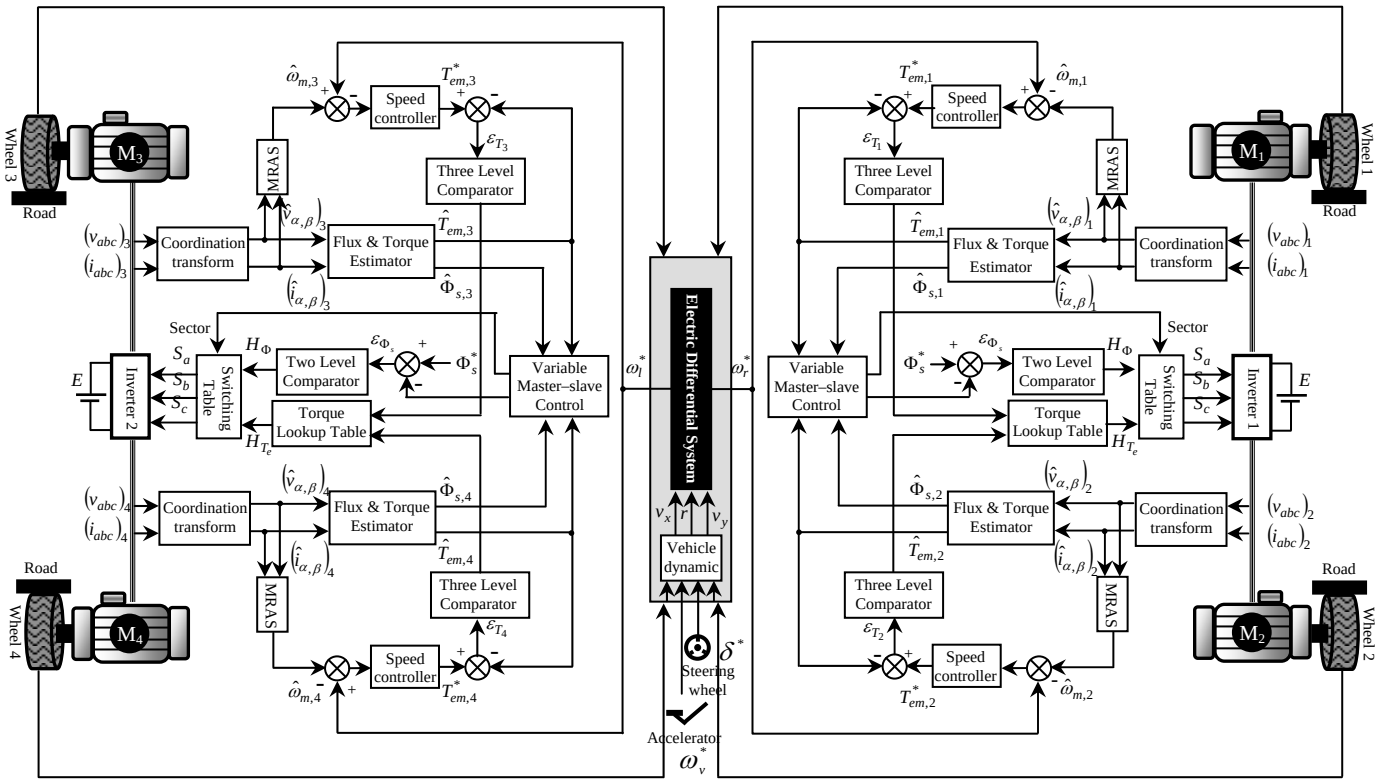

Fig. 16. Block diagram of the proposed electric differential based on a new master–slave DTC technique.

within 1 s because the gear ratio from the hand-steering wheel to the front driving wheels is approximately 10 s, and the maximum steering angles for both of the front wheels (assumed to be the same) can reach - 7°. Fig. 17(a) shows the longitudinal velocity of the vehicle v_x when the vehicle reaches a constant speed at 13 s. A delay in reaching this speed is allowed due to the acceleration of the vehicle mass. From Figs. 17(c) and (d), the lateral velocity v_y and the yaw moment r depend on the steering command of the driver. These two speeds occur only during cornering and they vanish when the vehicle is traveling on a straight road.

When the EV is driven by all four wheels in a cornering maneuver, the inner two wheels and the outer two wheels will have different rotational speeds, as shown in Figs. 17(g), (h), (i). This turn is assumed to be carried out at a constant speed. Figs. 17(e) and (f) illustrate the linear speeds of the wheels. It can be seen that a slight decrease occurs when the driver applies a steering command. However, the driver makes a steering angle which will be the steering angle of the front wheels. Thus, the electric differential immediately acts on the four motors simultaneously. This in turn lowers the speed of the inner two wheels in comparison with the outer two wheels. At such times, the speeds of the wheels change values. This affects the electrical and mechanical quantities, as shown in Figs. 17(s), (t), (u). During the first steering manoeuvers, the outer motors (M1 and M2) rotate at higher speeds than the inner motors (M3 and M4). When the speeds of the inner wheels are decreasing in accordance with their new references, the torque tries to change its sign because of the sudden change in speed [Figs. 17(j) and (k)]. Hence, the motors work in a braking mode by developing a negative torque. This working phase can be exploited for energy recuperation to the battery. The motors (M1 and M2) during the second steering maneuvers are presented in Figs. 17(r) and (i). In this case, the vehicle is turning on the left side at a speed of 30 km/h [Fig. 17(e)]. Despite the fact that the driving wheels are following different paths, they turn in the same direction with different speeds. The left driving wheels turn with less speed than the right wheels. The behavior of these speeds is illustrated in Figs. 17(h) and (i). When the speeds of the right wheels increase, the torque motors associated with these wheels increase and try to reach the growth of the speeds. Figs. 17(o) and (p) illustrate the variation in the electromagnetic torque of the motors. In the transient state, the torque is limited to 145 N.m.

The variation in the phase currents for each motor is presented in Figs. 17(l)-(o). Two intervals for the vehicle dynamics exist. The first interval occurs when the vehicle starts moving. In this interval, each motor solicits a high current to attain the reference speed imposed by the driver. This current is due to the starting torque caused by the vehicle inertia. The second interval starts after 17 s. In this interval, each motor tries to develop an electromagnetic

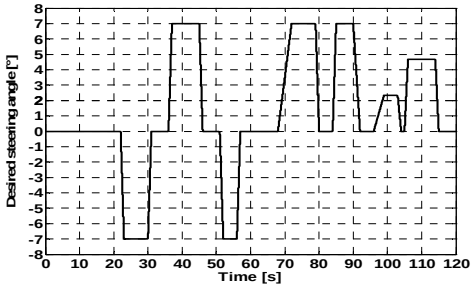
Desired steering angle [°]
Time [s]

(a)

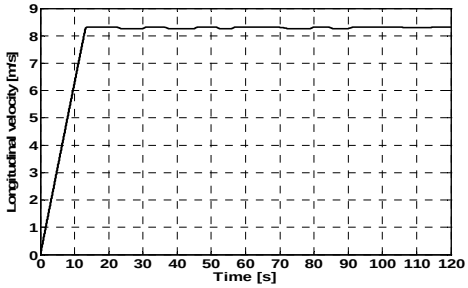
Longitudinal velocity [m/s]
Time [s]

(b)

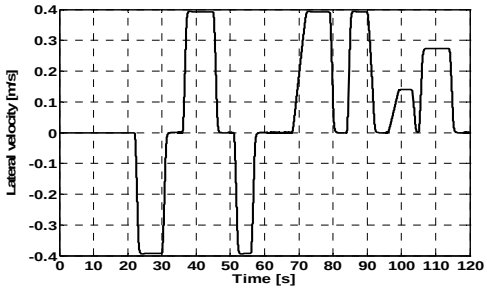
Lateral velocity [m/s]
Time [s]

(c)

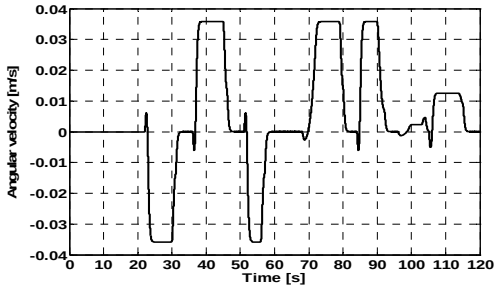
Angular velocity [m/s]
Time [s]

(d)

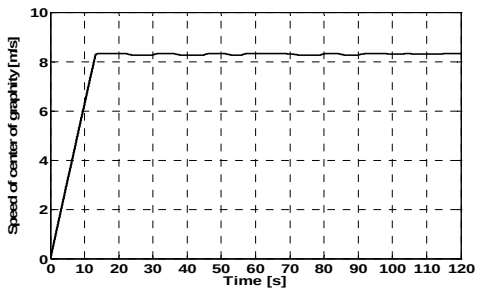
Speed of center of graphity [m/s]
Time [s]

(e)

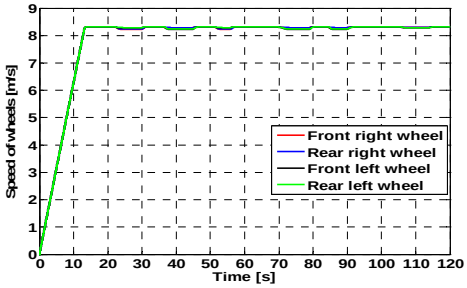
Speed of wheels [m/s]
Front right wheel
Rear right wheel
Front left wheel
Rear left wheel
Time [s]

(f)

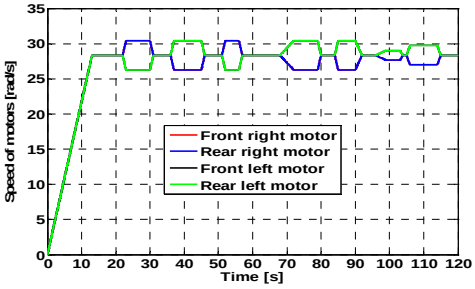
Speed of motors [rad/s]
Front right motor
Rear right motor
Front left motor
Rear left motor
Time [s]

(g)

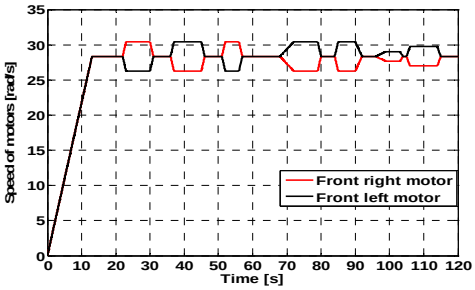
Speed of motors [rad/s]
Front right motor
Front left motor
Time [s]

(h)

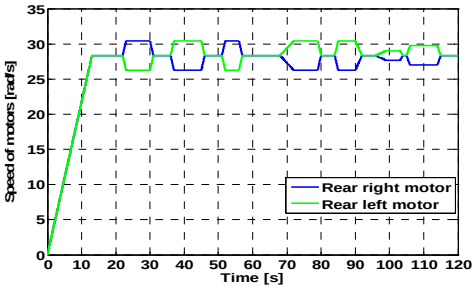
Speed of motors [rad/s]
Rear right motor
Rear left motor
Time [s]

(i)

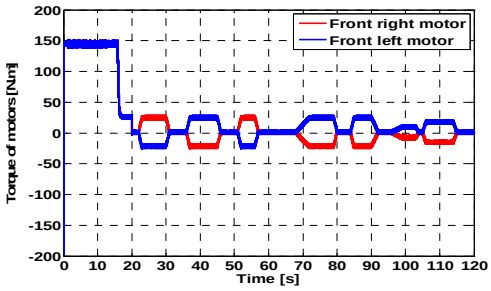
Torque of motors [Nm]
Front right motor
Front left motor
Time [s]

(j)

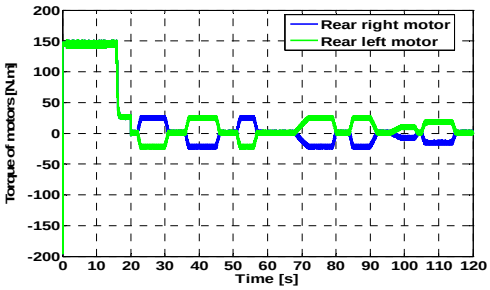
Rear right motor
Rear left motor
Torque of motors [N.m]
Time [s]

(k)

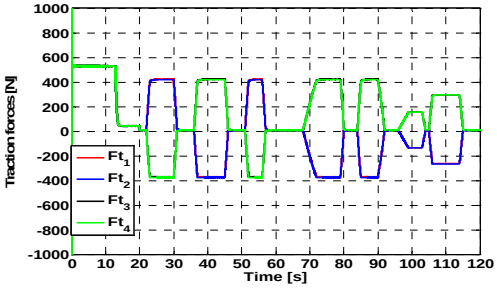
Ft1
Ft2
Ft3
Ft4
Traction forces [N]
Time [s]

(p)

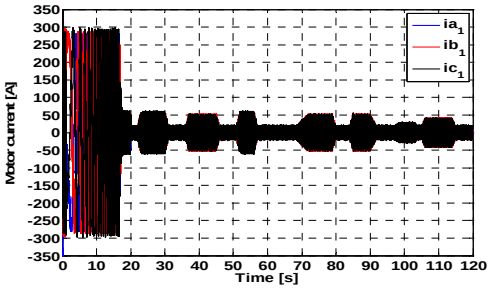
ia1
ib1
ic1
Motor current [A]
Time [s]

(l)

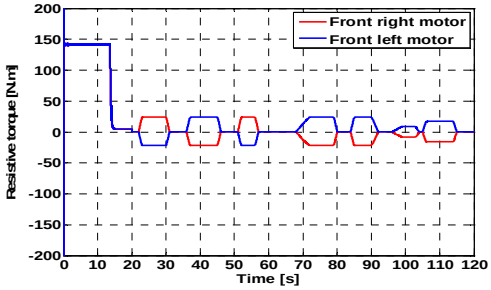
Front right motor
Front left motor
Resistive torque [N.m]
Time [s]

(q)

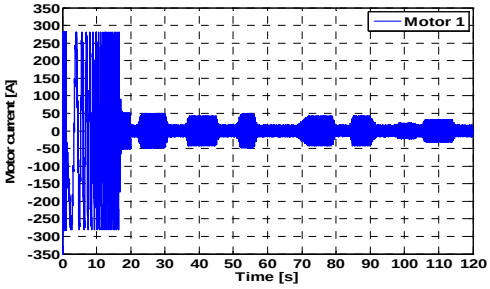
Motor 1
Motor current [A]
Time [s]

(m)

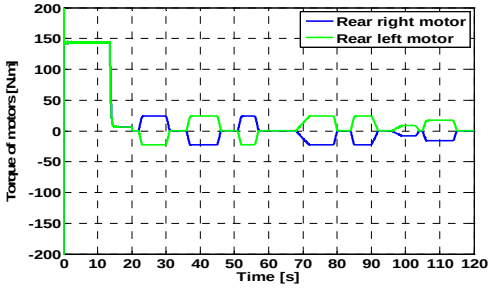
Rear right motor
Rear left motor
Torque of motors [N.m]
Time [s]

(r)

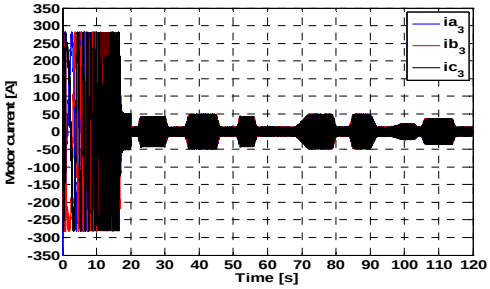
ia3
ib3
ic3
Motor current [A]
Time [s]

(n)

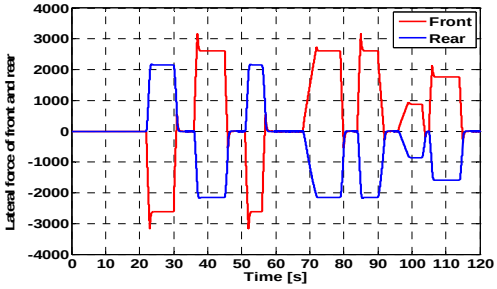
Front
Rear
Lateral force of front and rear
Time [s]

(s)

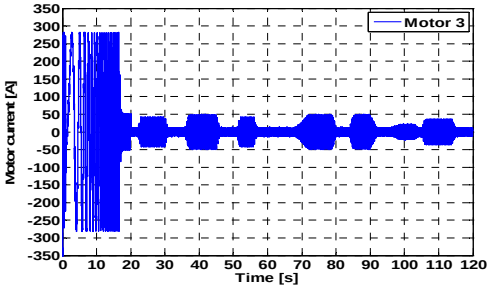
Motor 3
Motor current [A]
Time [s]

(o)

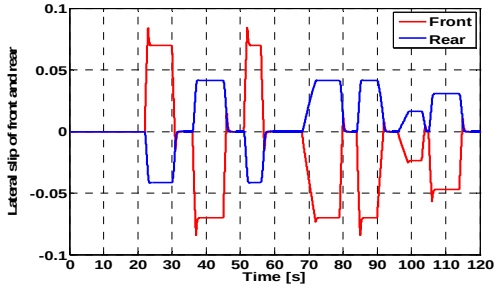
Front
Rear
Lateral slip of front and rear
Time [s]

(t)

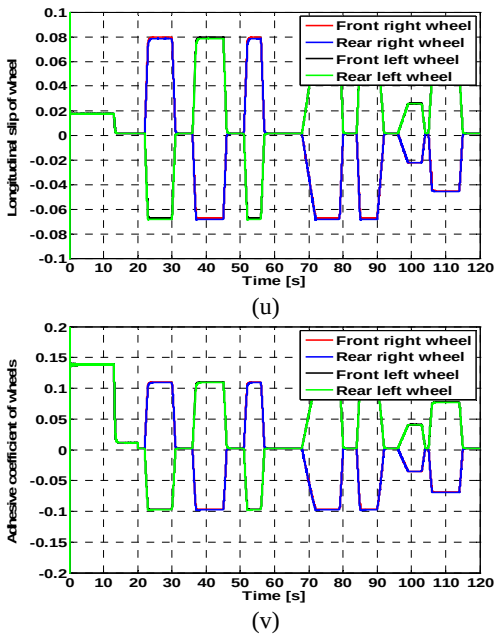

Fig. 17. Traction system behavior in a turn maneuver.

torque.

Fig. 17(p) illustrates the traction forces generated by the motors of the front axle (M1 and M3) and the motors of the rear axle (M2 and M4). High traction forces are provided by the motors to move the vehicle from a standstill. This phenomenon seems logical because these forces must overcome the overall forces resisting vehicle movement. A discrepancy exists between the traction forces during a movement through a turn. The motors located within the curvature of the turn produce lower traction forces than the motors that are outside the curvature of the turn. This scheme also applies to the load torques imposed on the motors, as shown in Figs. 17(q) and (r).

Fig. 17(p) shows the difference in traction forces of the motors during the completion of a turn. A difference is also observed for the speed of the motors [Fig. 17(g)] and the resistant torque of the motors [Fig. 17(q) and (r)]. When the speeds of the motors on the left side and right side diverge, the left wheels slow down, whereas the right wheels speed up to traverse the turn.

As shown in Fig. 17(s) and during the turn trajectory of the vehicle, the lateral forces applied to both the front and rear driving wheels show different values. The lateral side slip of the front and rear wheels are shown in Fig. 17(t). The behaviour of the lateral slip of the wheels is illustrated in Fig. 17(u). The longitudinal slips of the four wheels are maintained in the adhesive region. Fig. 17(v) shows that the adhesive coefficient of the outer driven wheels is larger than that of the inner wheels. Therefore, stability is maintained during vehicle turns. The simulation results validate the design of the electric differential under normal driving manoeuvres.

VI. Conclusion

In this study, a novel multi-machine control based on an electric differential system for EV applications is proposed. A new DTC algorithm is used to control the bi-machine traction system based on a speed MRAS observer. Simulation results shown that a vehicle with the proposed multi-machine robust control, which is composed of four in-wheel PMSMs, can successfully follow the trajectories defined by the steering maneuvers of a driver.

Appendix

TABLE I
Motor Parameters

Symbol	Quantity	Value
R_s	resistance	0,03 Ω
L_d	d-axis inductance	0,2 mH
L_q	q-axis inductance	0,2 mH
Φ_f	permanent magnet flux	0,08 Wb
p	pole pairs	4

TABLE II
Specification of the Vehicle Used in the Simulation

Symbol	Quantity	Value
M_v	vehicle mass	1562 kg
J_v	vehicle inertia	2630 kg.m²
J_ω	wheel inertia	1,284 kg.m²
L_f	distance from the CG to front axle	1,104 m
L_r	distance from the CG to rear axle	1,421 m
h_{cg}	heigh of the vehicle ctroid (CG)	0,5 m
S_f	frontal area of vehicle	2,04 m²
ρ	air density	1,2 kg.m^{-3}
C_{px}	drag coefficient	0,25
C_{rr}	rolling resistance coefficient	0,01
C_f	longitudinal stiffness of each tire lateral	37407 N/rad
C_r	lateral stiffness of each tire lateral	51918 N/rad
R_ω	wheel radius	0,294 m

References

[1] Y. Hori, “Future vehicles driver by electricity and control research on four wheel motored -UOT electric march II,” *IEEE Trans. Ind. Electron.*, Vol. 51, No. 5, pp. 954-962, Oct. 2004.

[2] A. Bouscaylor, B. Davat, B. de Fornel, B. Françis, “Multimachine multiconverter system: Application for electromechanical drives,” *European Physics Journal – Applied Physics*, Vol. 10, No. 2, pp. 131-147, May 2000.

[3] K. Matsuse, H. Kawai, Y. Kouno, and J. Oikawa, “Characteristics of speed sensorless vector controlled dual

induction motor drive connected in parallel fed by a single inverter," *IEEE Trans. Ind. Appl.*, Vol. 40, No. 1, pp. 153-161, Jan./Feb. 2004.
[4] Y. Zho, S. Li, X. Zhou, and Z. Fang, "The control strategy of electronic differentials for EV with four in-wheel motors," *IEEE Trans. Ind. Electron.* Vol. 51, No. 4, pp. 744-757, Aug. 2004.
[5] K. Hartani, M. Bourahla, Y. Miloud, and M. Sekour, "Direct torque control of an electronic differential for electric vehicle with separate wheel drives," *Journal of Automation & Systems Engineering*, Vol. 2, No. 2, pp. 15-26, Jun. 2008.
[6] E. Esmailzadeh, G. R. Vossoghi, and A. Goodarzi, "Dynamic modeling and analysis of a four motorized wheels vehicle," *Vehicle System Dynamics*, Vol. 35, No. 3, pp. 163-194, Mar. 2001.
[7] G. A. Magallan, C. H. D. Angelo, and G. O. Garcia, "Maximization of the traction force in a 2WD electric vehicle," *IEEE Trans. Veh. Technol.* Vol. 60, No. 2, pp. 369-380, Feb. 2011.
[8] S. Sakai, H. Sado, and Y. Hori, "Motion control in an electric vehicle with four independently driven in-wheel motors," *IEEE/ASME Trans. Mechatron.*, Vol. 4, No. 1, pp. 9-16, Mar. 1999.
[9] Y. P. Yang, Y. P. Luh, and C. H. Cheung, "Design and control of axial-flux brushless DC wheel motors for electric vehicles – Part I: Multiobjective optimal design and analysis," *IEEE Trans. Magn.*, Vol. 40, No. 4, pp. 1873-1882, Jul. 2004.
[10] Y. P. Yang, J. P. Wang, S. W. Wu, and Y. P. Luh, "Design and control of axial-flux brushless DC wheel motors for electric vehicles – Part II: Optimal current waveforms and performance test," *IEEE Trans. Magn.*, Vol. 40, No. 4, pp. 1883-1891, Jul. 2004.
[11] G. S. Buja and M. P. Kazmierkowski, "Direct torque control of PWM inverter-fed AC motors for EV with four in-wheel motors," *IEEE Trans. Ind., Electron.* Vol. 51, No. 4, pp. 744-757, Aug. 2004.
[12] M. A. Rahman and R. Qin, "A permanent magnet hysteresis hybrid synchronous motor for electric vehicles," *IEEE Trans. Ind. Electron.* Vol. 44, No. 1, pp. 46-53, Feb. 1997.
[13] K. Hartani and Y. Miloud, *Vehicle Stability Enhancement Control for Electric Vehicle Using Behaviour Model Control*, InTech, Chap. 6, pp. 127-158, 2011.
[14] K. Hartani, Y. Miloud, and A. Miloudi, "Improved direct torque control of permanent magnet synchronous electrical vehicle motor with proportional-integral resistance estimator," *Journal of Electrical Engineering & Technology*, Vol. 5, No. 3, pp. 451-461, Sep. 2010.
[15] K. Hartani, M. Bourahla, Y. Miloud, and M. Sekour, "Electronic differential with direct torque fuzzy control for vehicle propulsion system," *Turkish Journal of Electrical Engineering & Computer Sciences*, Vol. 17, No. 1, pp. 21-38 Mar. 2009.
[16] G. Wu and X. Xiao, "Speed controller of several of servo system based on MRAS method," *IEEE International Conference on Industrial Technology (ICIT)*, pp. 1-5, 2009.
[17] P. Vaclavek and P. Blaha, "Synchronous machine drive observability analysis and sensorless control design," *IEEE 2nd International Power and Energy Conference, PECon*, pp. 265-270, 2008.
[18] W. Maogang, Z. Rongxiang, and W. Junwei, "Sensorless estimation and convergence analysis based on MRAS for PMSM", *8th World Congress on Intelligent Control and Automation (WCICA)*, pp. 1641-1644, 2010.
[19] H. M. Kojabadi and M. Ghribi, "MRAS-based adaptive speed estimator in PMSM drives," *9th International Workshop on Advanced Motion Control*, pp. 569-572, 2006.
[20] K. Jinsong, Z. Xiangyun, W. Ying, and H. Dahing, "Study of position sensorless control of PMSM based on MRAS," *IEEE International Conference on Industrial Technology (ICIT)*, pp. 1-4, 2009.
[21] A. Quntao and S. Li, "On-line parameter identification for vector controlled PMSM drives using adaptive algorithm," *IEEE Vehicle Power and Propulsion Conference*, pp. 1-6, 2008.
[22] P. M. Kelecy and R. D. Lorenz, "Control methodology for single inverter, parallel connected dual induction motor drives for electric vehicles," *Power Electronics Specialists Conference, PESC'94, 25th Annual IEEE*, Vol. 2, pp. 987-991, 1994.
[23] D. Bidart, M. Pieterzak-David, M. Fadel, and P. Maussion, "Mono interver dual parallel PMSM structure and control strategy," *34th Annual Conference of IEEE Industrial Electronics (IECON)*, pp. 3073-3078, 2008.
[24] D. Bidart, M. Pieterzak-David, and M. Fadel, "Mono inverter multi parallel PMSM-structure and control strategy," *IET Electric Power Applications.* Vol. 5, No. 3, pp. 288-294, Mar. 2011.
[25] J. Chiasson, D. Seto, F. Sun, A. Stankovic, and S. Bortoff, "Independent control of PM motor using a single inverter: application to elevator doors," *IEEE American Control Conference Proceedings*, pp. 093-3098, 2002.
[26] M. Shibata and N. Hoshi, "Novel inverter topologies for two-wheel drive electric vehicles with two permanent magnet synchronous motors," *European Conference on Power Electronics and Applications*, pp. 1-10, 2007.
[27] H. Mokhtari and A. Alizadeh, "A new multi-machine control system based on direct torque control algorithm," *7th International conference on Power Electronics, ICPE'07*, pp. 1103-1108, 2007.
[28] N. Kanghyun, O. Sehoon, F. Hiroshi, and H. Yoichi, "Estimation of sideslip and angles of electric vehicles using lateral tire force sensors through RLS and Kalman Filter Approaches," *IEEE Trans. Ind. Electron.* Vol. 60, No. 3, Mar. 2013.
[29] G. Genta, *Motor Vehicle Dynamics: Modeling and Simulation, Series on Advances in Mathematics for Applied Sciences*, World Scientific Publishing Co. Inc., Vol. 43, 1997.
[30] T. D. Gillespice. "Fundamentals of vehicle dynamics," *Society of Automotive Engineers Inc.*, 2014.
[31] M. Sekour, K. Hartani, and A. Draou, "Sensorless fuzzy direct torque control for high performance electric vehicle with four in-wheel motors," *Journal of Electrical Engineering & Technology*, Vol. 8, No. 1, pp. 123-132, Jan. 2013.
[32] H. B. Pacejka and E. Bakker, "The magic formula tyre model," *Vehicle System Dynamics*, Vol. 21, No. 1, pp. 1-18, 1992.
[33] H. B. Pacejka, *Tire and Vehicle Dynamics*, 2nd ed., Butterworth-Heinemann, pp. 165-166, 2006.
[34] Y. Y. Wong, *Theory of Ground Vehicles*, Wiley, 2008.
[35] R. Rajamani, *Vehicle Dynamics and Control*, Springer-Verlag, 2006.

Kada Hartani was born in Saida, Algeria, in 1976. He received his B.S. degree in Electrotechnical Engineering, in 1997. He also received his M.S. degree and his Ph.D. degree in Electrical Control from the University of Sciences and Technology of Oran (USTO), Oran, Algeria, in 2003 and 2007, respectively. He is presently working as a Professor at the University of Saida, Saida, Algeria. His current research interest include multi-machine multi-converter systems, antilock braking systems, traction control systems, and anti-skid control for electric vehicles.

Abdelader Merah was born in Saida, Algeria, in 1983. He received his B.S. degree in Automatic Engineering from the University of Sciences and Technology of Oran (USTO), Oran, Algeria, in 2007, and his M.S. degree from the University of Saida, Saida, Algeria, in 2012, where he is presently working toward his Ph.D. degree. His current research interests include the analysis and intelligent control of electrical machines and automotive control.

Azeddine Draou was born in Maghnia, Algeria. He received his B.S. degree from the University of Sheffield, Sheffield, England, UK, in 1980, his M.S. degree from Aston University, Birmingham, England, UK, in 1981, and his Ph.D. degree from the Tokyo Institute of Technology, Tokyo, Japan, in 1994, all in Electrical Engineering. From 1982 to 1986, he was a Senior Engineer at the Sonatrach Ammonia Plant, Arzew, Algeria. In 1986, he became a Lecturer in the Department of Electrotechnics, University of Sciences and Technology of Oran (USTO), Oran, Algeria. He was promoted to Assistant Professor, in 1989, and an Associate Professor, in 1996, and a Professor in 2014. He is currently on leave from this university. He has published over 130 papers in technical journals and conference proceedings. He was also a contributing author of the *Power Electronics Handbook* edited by Dr. M. H. Rashid, Academic Press, San Diego, in 2001. In 1994, he received an IEE Japan medal for the annual meeting. His current research interests include power electronics applied to electric vehicle, static VAR compensation, multilevel inverters, and the intelligent control of AC drives, microgrid systems, distributed energy resources, UPFC and FACTS devices. Dr. Draou is a Senior Member of the IEEE/ P.E.S, I.E.S, I.A.S societies.